THE JOURNAL OF PHYSICAL CHEMISTRY C

ARTICLE

pubs.acs.org/JPCC

In Situ High-Pressure and Low-Temperature Study of Ammonia Borane by Raman Spectroscopy

Ang Liu and Yang Song*

Department of Chemistry, The University of Western Ontario, London, Ontario N6A 5B7, Canada

ABSTRACT: As a promising hydrogen storage material, ammonia borane was investigated at simultaneous high pressures (up to 15 GPa) in a diamond anvil cell and at low temperatures (down to 80 K) using a cryostat by in situ Raman spectroscopy. When ammonia borane was cooled from room temperature to 220 K at near ambient pressure, an expected phase transformation from *I*4*mm* to *Pmn*2$_1$ was observed. Then the sample was compressed to 15 GPa isothermally at 180 K. Three pressure-induced structural transformations were observed as evidenced by the change in the Raman profile as well as the pressure dependence of the major Raman modes. The decompression and warming-up experiments suggest that these pressure−temperature (P−T)-induced transformations are reversible. These observations, together with factor group analysis, allowed us to examine the possible structures of the new high-pressure phases and the nature of phase transitions. Raman measurements from multiple runs covering various P−T paths, when combined with previously established room-temperature and high-pressure data, enabled the updating of the P−T phase diagram of ammonia borane in the pressure region of 0−15 GPa and the temperature region of 80−350 K.

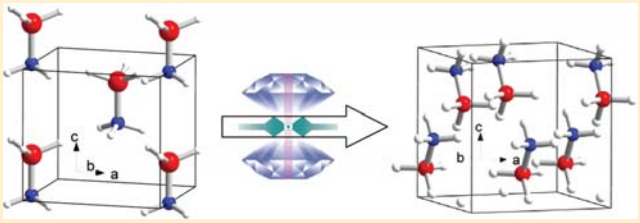

INTRODUCTION

As a potential hydrogen storage material, ammonia borane (NH_3BH_3) has received extensive investigation among many solid-state chemical hydrides over the past few decades.[1−4] Ammonia borane is a lightweight molecular complex with a high hydrogen content (19.6 wt %) that exceeds the 2015 U.S. Department of Energy target (9 wt %) for on-board hydrogen storage systems.[5] Consequently, substantial research efforts were made toward the understanding of hydrogen chemistry involving ammonia borane and related B−N compounds.[2,4,6−9] The hydrogen release mechanism has been extensively studied for ammonia borane, and it was found that the three thermolysis steps required different high temperatures and exhibited very slow kinetics.[2,3] Therefore, the hydrogen storage application using ammonia borane and its derivatives has been examined with an extended list of materials and conditions. For instance, a class of composition modified ammonia borane derivatives, such as alkali-metal amidoboranes, was found to release hydrogen at relatively lower temperatures.[8−10] More recently, Li et al. showed that hydrogen can be released from ammonia borane confined in the metal−organic framework with enhanced kinetics and at lower temperatures (e.g., ∼30 °C).[7]

The structures of ammonia borane have been studied using X-ray diffraction, neutron diffraction, and theoretical calculations under ambient conditions or at low temperatures.[10−19] Under ambient conditions, ammonia borane adopts the disordered body-centered tetragonal structure (space group *I*4*mm* with two molecules per unit cell, Figure 1a) with cell parameters a = 5.255 and c = 5.048 Å.[17] At low temperatures, an ordered orthorhombic structure (space group *Pmn*2$_1$ with two molecules per unit cell, Figure 1b) with cell parameters a = 5.517, b = 4.742, and c = 5.020 Å was identified by Bowden et al.[16] using X-ray diffraction at 90 K and by Klooster et al.[18] using single crystal neutron diffraction at 200 K. In their studies, the unconventional dihydrogen bonding was reinforced due to the strong dipole−dipole intermolecular interactions and the short distances between the hydrogen atoms with N−H being the proton donor and H−B being the proton acceptor.[16,18]

The application of high pressure to materials may induce significant changes in molecular structures and associated properties, such as enhanced hydrogen storage capacities, and therefore, a wide range of hydride complexes (e.g., ammonia borane, diborane, calcium borohydride, and sodium amide) as potential hydrogen storage materials have been investigated under high pressures.[20−24] Using vibrational spectroscopy, X-ray diffraction, and neutron diffraction as well as ab initio calculations, in particular, ammonia borane has been extensively studied under high-pressure conditions as well.[24−31] Early spectroscopy studies demonstrated that NH_3BH_3 undergoes two phase transitions upon compression to 40 kbar.[25,26] Later, Lin et al.[27] and Xie et al.[24] performed independent high-pressure studies on ammonia borane up to 20 GPa using Raman spectroscopic and combined Raman/IR spectroscopy,

Special Issue: Chemistry and Materials Science at High Pressures Symposium

Received: June 24, 2011
Revised: October 6, 2011
Published: October 26, 2011

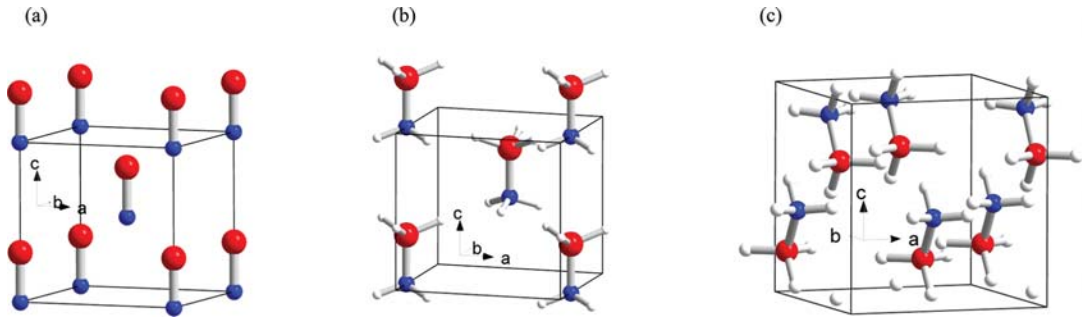

Figure 1. Known crystal structures of NH_3BH_3 at ambient pressure and room temperature (space group *I4mm*) (a), at ambient pressure and <225 K (space group $Pmn2_1$) (b), and above 1.5 GPa and room temperature (space group $Cmc2_1$) (c). The coordinate system is indicated to show the orientations of the unit cell. The red, blue, and while balls denote boron, nitrogen, and hydrogen atoms, respectively. Due to the orientational disorder along the B−N molecular axis in (a), the hydrogen atoms are not shown.

respectively, and similar new phase transitions were found in the higher pressure regions in both studies. The crystal structures of these new high-pressure phases were subsequently examined by X-ray diffraction measurements and theoretical calculations by Filinchuk et al.[28] and Chen et al.[29] They consistently established that at room temperature and above 1.5 GPa, NH_3BH_3 crystallizes into a new ordered orthorhombic structure (space group $Cmc2_1$ with four molecules per unit cell, Figure 1c). Further high-pressure X-ray and neutron diffraction experiments and density functional theoretical calculations confirmed these observations but also proposed a new triclinic structure with space group *P*1 above 8 GPa.[30] Most recently, Wang et al.[31] investigated the structural and dynamical properties of ammonia borane at high pressures up to 60 GPa by molecular dynamics simulations, which helped with the understanding of the relationship and the transformation mechanism among the three known phases of ammonia borane.

Furthermore, the pressure-induced formation of novel hydrogen complexes has demonstrated strong promise in the development of new hydrogen storage materials.[32−37] Especially for ammonia borane, for instance, the significant abundance of hydrogen content (8−12 wt % H_2) in the ammonia borane−hydrogen complexes $[NH_3BH_3\cdot(H_2)_x]$ formed under high pressures shows great potential for using ammonia borane as a possible hydrogen storage material in an alternative way.[33,34,36] For practical applications, it would be desirable to recover the hydrogen complexes under near ambient conditions. Indeed, a previous high-pressure study of hydrogen clathrate hydrate formed under high pressures indicated that the complex can be quenched to ambient pressure, but only at low temperatures (e.g., <145 K).[35] Therefore, it is of great interest to explore the structures and properties of ammonia borane in a wider $P-T$ range, especially in the low-temperature region as well as the reversibility of pressure-induced structural changes at low temperatures. Temperature-induced phase transitions have been observed previously using Raman spectroscopy, but only at ambient pressure.[19] Here we report the first simultaneous high-pressure and low-temperature experiments on ammonia borane using Raman spectroscopy up to 15 GPa and down to 80 K. We found interesting new $P-T$ induced transformations, and these observations provide a more in-depth understanding of the structures and properties of ammonia borane that are important for hydrogen storage applications.

EXPERIMENTAL SECTION

White ammonia borane powders (97%) were purchased from Sigma-Aldrich and used without further purification. Their identity and purity were confirmed by comparing the observed Raman spectrum with that from ref 24. A symmetric diamond anvil cell (DAC) equipped with a pair of type I diamonds with 300 μm culets was used for the high-pressure experiments. This DAC made of BeCu was specially designed to allow its use in a cryostat for in situ low-temperature measurements. A tungsten gasket was preindented to 50 μm, and a hole with 100 μm diameter was drilled at the center as the sample chamber. The sample was loaded into the DAC in an MBraun LABmaster glovebox to accommodate the hygroscopicity of the sample. The nitrogen atmosphere in the glovebox was maintained at <10 ppm H_2O and O_2 during the loading of the sample. For the same reason, no fluid pressure transmitting medium was used. A few ruby chips were placed inside the sample chamber as the pressure calibrant. To calibrate the temperature effects on the ruby fluorescence lines, we loaded additional ruby chips outside the sample chamber onto the back surface of the diamond as the ambient-pressure reference. The pressure was determined using the R_1 fluorescence line by fitting the simultaneous pressure and temperature dependence that was established previously by Ragan et al.[38] and Yen et al.[39] The ruby spectral profiles showed no significant nonhydrostatic effects, particularly in the lower pressure regions (e.g., <10 GPa) at low temperatures.

To achieve simultaneous high-pressure and low-temperature conditions, we used a customized cryogenic station designed and constructed by Cryo Industries, Inc. The cryostat contained a compact vacuum chamber that housed the DAC anchored by a cold collar. A vacuum of 1×10^{-7} Torr was maintained in the cryostat chamber by a turbopump to ensure the thermal insulation between the sample and the environment. Liquid nitrogen as the cryogen was introduced via an internal loop through the cold collar that allowed the effective cooling of the DAC conductively down to 77 K. Two silicon dioxide sensors were placed in different locations: one on the cold collar and one on the diamond seat (made of tungsten carbide). The temperature was measured and controlled by the Cryo-con temperature controller from Cryogenic Control System, Inc. with an accuracy of ±1 K. The temperature readings from the two sensors suggested a maximum temperature gradient of 1 K. The cryostat was equipped with two panels with different optical windows. For the Raman measurements, the front window material was fused silica,

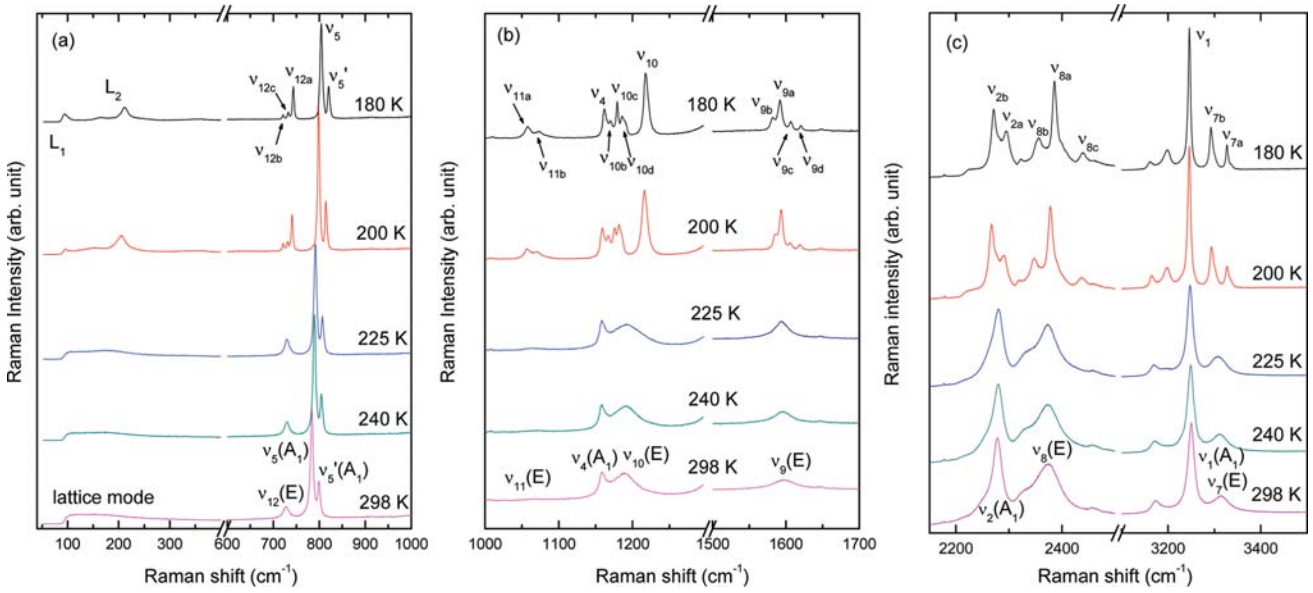

Figure 2. Selected Raman spectra of NH_3BH_3 collected at ambient pressure from 298 to 180 K in the region of 50−1000 cm^{-1} (a), 1000−1700 cm^{-1} (b), and 2150−3500 cm^{-1} (c). The relative intensities are normalized and thus are directly comparable. The temperatures are labeled for each spectrum. The assignments are labeled for each Raman mode at 298 and 180 K (see Table 1).

while the back window could be any transparent material for illumination purposes. In addition, the back panel had a feedthrough housing four retractable hex-keys that could be engaged with the screws on the DAC inside the cryostat. Twisting these keys would allow the change of pressure at low temperatures in situ.

Raman measurements were carried out with a customized Raman microspectroscopy system accommodating the operation of the cryostat. A 488 nm blue laser produced by Innova Ar^+ laser (Coherent Inc.), which was used as the excitation source, was focused on the sample through the optical windows on the front panel of the cryostat by a 10× Mitutoyo objective. The scattered Raman light was dispersed by a SpectroPro spectrometer, and collected by a liquid-nitrogen-cooled charge-coupled device (CCD) detector, both from Acton. Rayleigh scattering was removed by a pair of notch filters that enabled a spectral range >100 cm^{-1} to be measured. A grating with 1800 lines/mm was used achieving a resolution of 0.1 cm^{-1}. Neon lines were used for the spectral calibration of the system with an uncertainty of ±1 cm^{-1}.

In the experiments, we designed different pressure−temperature ($P-T$) paths each with multiple runs to ensure the reproducibility. Initially, we examined the temperature effects by cooling the sample from room temperature to 80 K at ambient pressure as well as at the highest pressure, 15.94 GPa. Then to investigate the pressure effects at low temperatures, we compressed the sample up to 15.94 GPa isothermally at 180 K. Finally, we performed the decompression and the warming up procedures to check the reversibility of the transformations.

RESULTS AND DISCUSSION

Raman spectra of ammonia borane were collected under ambient conditions as a starting point and are shown at the bottom of Figure 2. At ambient pressure and temperature, ammonia borane has a C_{3v} molecular symmetry and a C_{4v} factor group symmetry (for space group $I4mm$). Thus, the irreducible representations for Raman active modes are[19]

$$\Gamma^{I4mm}_{\text{internal}} = 5A_1 + 6E \quad (1)$$

$$\Gamma^{I4mm}_{\text{lattice}} = E \quad (2)$$

where the A_2 mode is omitted from the above representations since it is not Raman active. Therefore, the assignment of the observed Raman modes can be made by adopting the previous work[19,24] as shown in Table 1.

A. Raman Spectra during Cooling down to 180 K. Raman spectra were collected as a function of temperature from 298 to 180 K at near ambient pressure. Selected Raman spectra from the cooling sequence are depicted in Figure 2. The significant sharpening of the lattice modes as well as the characteristic splitting of the internal modes with E symmetry were observed when the temperature was lowered to <220 K. For example, two new lattice modes (L_1 and L_2) appeared at 94 and 212 cm^{-1}, which became much sharper and more pronounced, indicating the transition into a new crystal structure. In addition, the doubly degenerate modes (e.g., the NBH rocking mode ν_{12} and ν_{11}, the BH_3 deformation mode ν_{10}, the NH_3 deformation mode ν_9, the asymmetric B−H stretching mode ν_8, and the asymmetric N−H stretching mode ν_7) all split into two to four components (Figure 2 and Table 1). Noticeably, the low temperature (220 K) also induced the splitting in the symmetric B−H stretching mode, ν_2 (A_1). These obvious changes collectively suggested a phase transition below 225 K, consistent with the previous observations by Hess et al.[19] The labeling of the new components of the Raman modes as a result of the splitting at low temperatures follows the convention that the original and the most prominent peak is assigned as ν_a, whereas all the other affiliated components are assigned based on their appearing sequence (e.g., as ν_b, ν_c, ν_d, etc.).

B. Raman Spectra on Compression to 15.92 GPa at 180 K. *B1. Lattice Region.* (Figure 3a). Upon compression to 1.5 GPa, three new lattice modes (labeled as L_3, L_4, and L_5) were observed

dx.doi.org/10.1021/jp205962g |J. Phys. Chem. C 2012, 116, 2123–2131

Table 1. Assignments and Vibrational Frequencies (cm^{-1}) of Observed Raman Modes of NH_3BH_3 at Ambient Pressure and Different Temperatures

this work		reference[a]			
room temp	180 K	298 K	224 K	88 K	description
3314 $\nu_7(E)$	3327 ν_{7a}	3316	3327	3338	asym. N−H stretch
				3331	
	3292 ν_{7b}		3302	3300	
				3290	
3250 $\nu_1(A_1)$	3246 ν_1	3250	3249	3247	sym. N−H stretch
				3240	
3172	3198	3176	3199	3202	overtone?
	3161		3171	3165	
2375 $\nu_8(E)$	2439 ν_{8c}		2413	2434	asym. B−H stretch
				2400	
	2386 ν_{8a}	2375	2371	2373	
	2356 ν_{8b}			2356	
			2340	2343	
2278 $\nu_2(A_1)$	2295 ν_{2a}	2279	2280	2289	sym. B−H stretch
	2271 ν_{2b}		2263	2263	
1596 $\nu_9(E)$	1620 ν_{9d}		1615	1622	NH_3 deformation
	1606 ν_{9c}			1609	
	1592 ν_{9a}	1600	1595	1593	
	1582 ν_{9b}			1585	
1189 $\nu_{10}(E)$	1217 ν_{10a}	1189	1209	1214	BH_3 deformation
	1186 ν_{10d}		1178	1180	
	1179 ν_{10c}			1173	
	1170 ν_{10b}		1164	1166	
1158 $\nu_4(A_1)$	1162 ν_{4a}	1155	1156	1157	BH_3 deformation
			1080	1086	NBH rock
1067 $\nu_{11}(E)$	1073 ν_{11b}	1065	1066	1073	
	1058 ν_{11a}		1062	1056	
799 $\nu_5'(A_1)$	820 ν_5'	800	804	813	^{10}B−N stretch
				810	
				798	
784 $\nu_5(A_1)$	804 ν_5	784	789	794	^{11}B−N stretch
728 $\nu_{12}(E)$	743 ν_{12a}	727	734	740	NBH rock
	733 ν_{12c}		727	731	
	722 ν_{12b}		723	721	
124 L	212 L_2				lattice mode
	94 L_1				

[a] Reference 19.

with a concurrent vanishing of the two original lattice modes, L_1 and L_2. This observation, together with the very sharp and intense new lattice mode L_4 at 178 cm^{-1}, indicated a major phase transition into a new ordered crystal structure. This new phase spans in the pressure region of 1.5−5.0 GPa as suggested by the similar Raman profiles in this region. Above 5.0 GPa, the L_3 and L_5 modes gradually diminished and completely vanished above 8.0 GPa. Concurrently, a significant band broadening was observed above 8.0 GPa, suggesting another phase transition, possibly to a more disordered structure. Compared with the previous high-pressure studies of ammonia borane at room temperature,[24] the Raman profiles observed here were quite similar, except that more lattice modes were observed in the lower pressure region (i.e.,1.5−5.0 GPa) but fewer in the higher pressure regions (i.e., >5.0 GPa).

B2. NBH Rocking Regions. (Figure 3b,c). There are two NBH rocking modes: the low-frequency mode ν_{12} (700−850 cm^{-1}) and the high-frequency mode ν_{11} (1025−1150 cm^{-1}). The changing of the ν_{12} mode from a triplet to a new blue-shifted doublet, together with the abrupt changing of the Raman shift and the broadening of the ν_{11} modes, strongly suggested a phase transition at 1.5 GPa. Upon further compression, the disappearance of the doublet ν_{12} mode and the gradual development of the ν_{11} mode into a prominent triplet at 5.0 GPa clearly signified another phase transition at this pressure. When compressed to above 8.0 GPa, the ν_{12} mode totally faded away while there was a dramatic reduction in the intensities of the ν_{11} modes, implying a third phase transformation, as was consistently indicated by the lattice profiles.

B3. BH_3 and NH_3 Deformation Regions. (Figure 3c,d). There are two BH_3 deformation modes in the region of 1100−1300 cm^{-1}, i.e., ν_4 and ν_{10} modes, and one degenerate NH_3 deformation mode, ν_9, in the region of 1500−1650 cm^{-1}. As the pressure was increased to above 1.5 GPa, the ν_{10} mode was strongly perturbed: it first red-shifted abruptly by −23 cm^{-1} and subsequently developed into a doublet, for example, at 2.74 GPa. In contrast, the ν_9 mode exhibited a blue shift and merged from a quartet into a doublet. All this evidence suggests the first phase transformation took place at 1.5 GPa as was indicated by the other modes. The ν_{10a} mode exhibited another abrupt red shift above 5.0 GPa, at which pressure the intensity of the two components of the ν_9 mode switched. Beyond 8.0 GPa, the ν_{10} modes split into a triplet, whereas the ν_4 mode was almost indiscernible. All of these observations corroborate the two additional phase changes, which took place at 5.0 and 8.0 GPa, respectively.

B4. B−H and N−H Stretching Regions. (Figure 3e,f). The Raman features in the stretching regions resembled the other regions described above. In particular, the multiple components of the symmetric B−H stretching ν_2 mode merged into a single prominent band, while the asymmetric B−H (N−H) stretching mode ν_8 (ν_7) evolved from triplet (doublet) into new convoluted patterns at 1.5 GPa. Above 5.0 GPa, the doublet ν_7 mode further merged into a single mode, consistent with the proposed second phase transition. Furthermore, the significant merging of all the ν_8 components suggested a third phase transition above 8.0 GPa.

C. Pressure Effects on Raman Modes. The phase transition boundaries suggested by the Raman features described above can be better visualized by examining the pressure dependences of the characteristic Raman modes (as shown in Figure 4). Pressure coefficients ($d\nu/dP$) were calculated by fitting the quadratic (<1.5 GPa) or linear (1.5−15.94 GPa) regressions of the original experimental data. The different types of regression functions needed in different pressure regions suggest different pressure behavior (e.g., compressibility) of NH_3BH_3, which has been observed in other hydride complexes such as $NaNH_2$,[20] where quadratic functions were also used to fit the Raman modes in an intermediate high-pressure region. As can be seen in Figure 4, three distinct pressure regions with possibly different phases could be inferred by the sharp changes in the pressure dependence. These pressure coefficients are larger in the second (1.5−5.0 GPa) and fourth (>8.0 GPa) phases while they are relatively smaller in the other two phases (i.e., <1.5 GPa and 5.0−8.0 GPa), indicating the different compressibilities of these

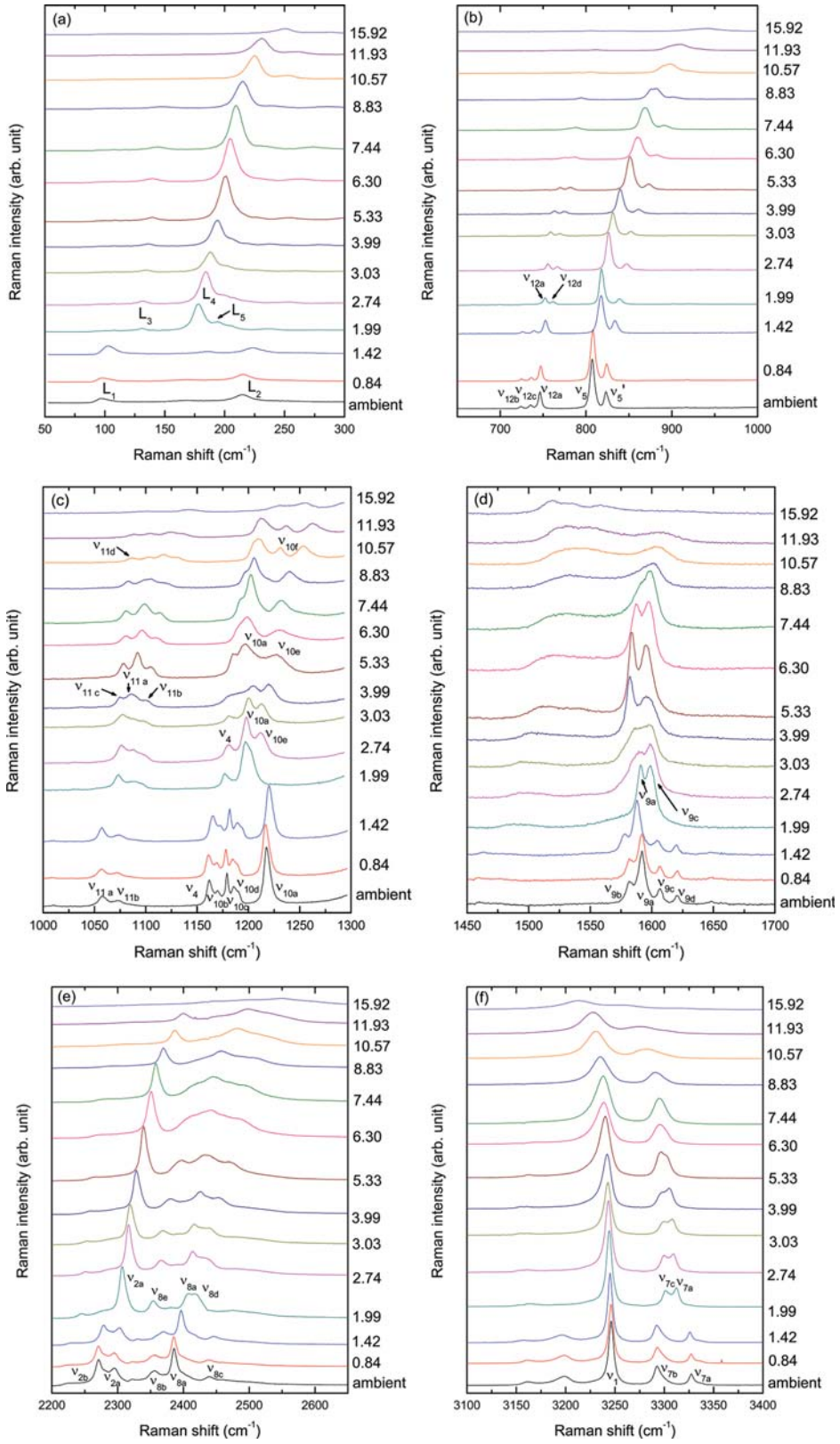

Figure 3. Selected Raman spectra of NH_3BH_3 collected on compression up to 15.92 GPa at 180 K in the region of 50−300 cm^{-1} (a), 600−1000 cm^{-1} (b), 1000−1300 cm^{-1} (c), 1450−1700 cm^{-1} (d), 2200−2700 cm^{-1} (e), and 3100−3400 cm^{-1} (f). The relative intensities are normalized and thus are directly comparable. The units of the pressures are in gigapascals for each spectrum. The assignments are labeled for selected Raman mode at selected pressures (see Table 1).

dx.doi.org/10.1021/jp205962g |J. Phys. Chem. C 2012, 116, 2123–2131

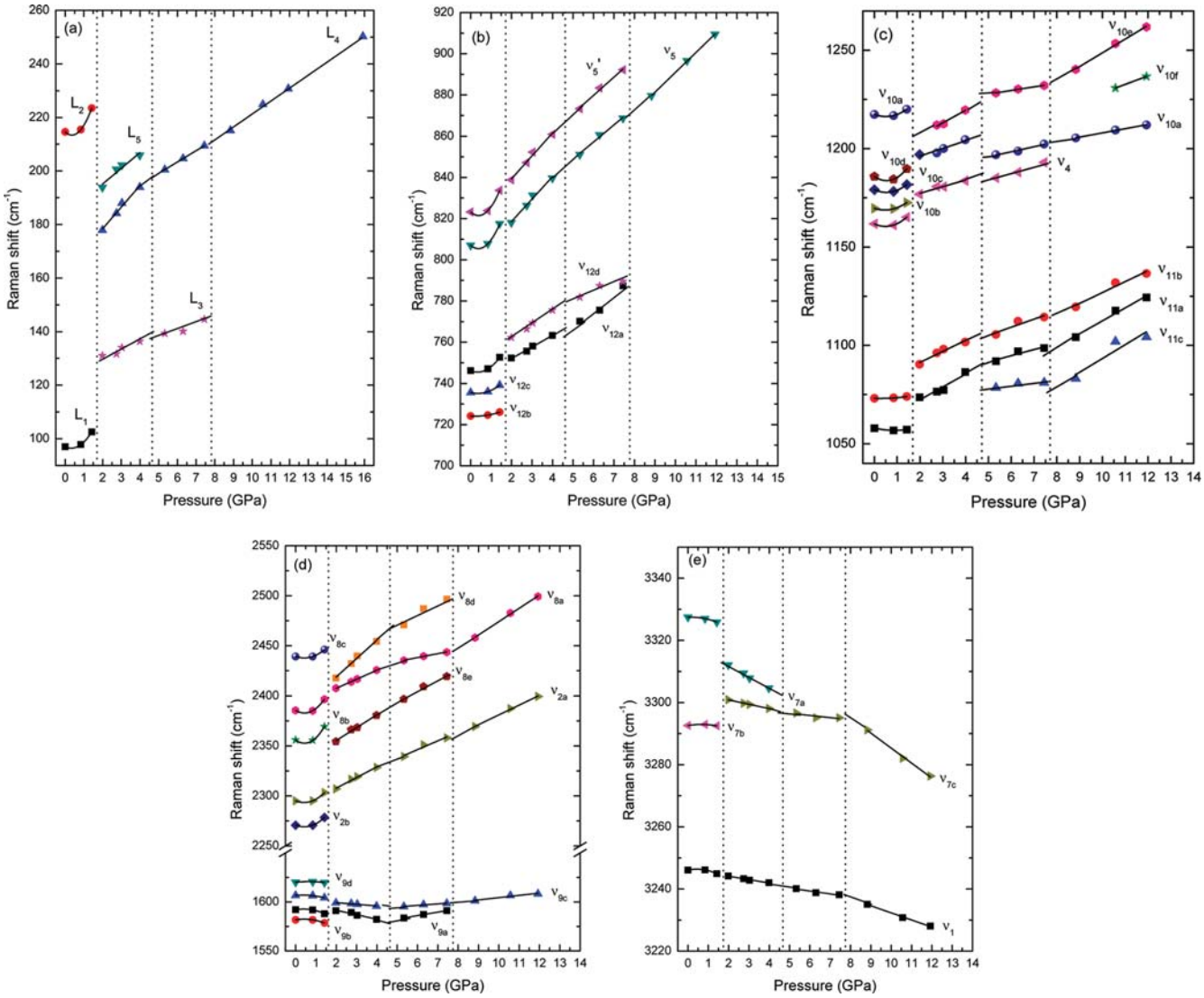

Figure 4. Pressure dependence of Raman modes of NH_3BH_3 on compression at 180 K. Different symbols represent Raman modes with different origins. The solid lines crossing the solid symbols are based on linear regression. The vertical dashed lines indicate the proposed phase boundaries.

phases. Generally speaking, most of the Raman modes displayed the pressure-induced blue shifts due to the stiffening of most bonds of ammonia borane. However, the N−H stretching modes, such as the ν_7 and ν_1 modes, have conspicuously negative slopes (e.g., −1.39, −0.71, and −4.81 cm^{-1} GPa^{-1} for the ν_7 mode in the three high-pressure regions, respectively). More interestingly, both components of the ν_9 mode exhibited a change of the sign of the pressure coefficient, from negative to positive across the phase boundary at 5 GPa. The soft behavior of these Raman modes could be explained by the weakening of the N−H bond and the strengthening of the dihydrogen bond by compression.[24,27,31] All of these observations are consistent with our previous high-pressure Raman measurements on ammonia borane taken at room temperature.[24]

D. Raman Spectra upon Decompression and Warming up. To better understand the combined low-temperature and high-pressure effects on ammonia borane as well as the reversibilities of the observed transitions, the experiments were carried out by decompression and warming up as well. However, it is difficult to strictly follow an isobaric or an isothermal path due to the correlation of the pressure and temperature, a mechanical response from the cell. As a result, after the lowest temperature of 80 K and the highest pressure of 15.94 GPa were achieved, Raman measurements were collected on simultaneous decompression and warming up, with selected spectra shown as they were in Figure 5. At 3.43 GPa and 165 K, for instance, both the lattice modes and the other internal modes were recovered to resemble the initial pattern at 180 K and 1.5 GPa in the same phase region. Similarly, the Raman pattern observed at 1.21 GPa and 220 K upon decompression and warming up was almost identical to the initial spectrum taken under similar $P-T$ conditions. Therefore, all the phase transitions were reversible with very little hysteresis upon decompression and warming up.

E. Discussion. Our Raman measurements of NH_3BH_3 on compression at 180 K as well as the pressure dependence of the characteristic Raman modes collectively suggested three pressure-induced phase transitions at 1.5, 5, and 8 GPa at 180 K. We note that these transition boundaries were very well aligned with those observed at room temperature in our previous study,[24] i.e., at about 2, 5, 8, and 10 GPa. However, the starting structure in

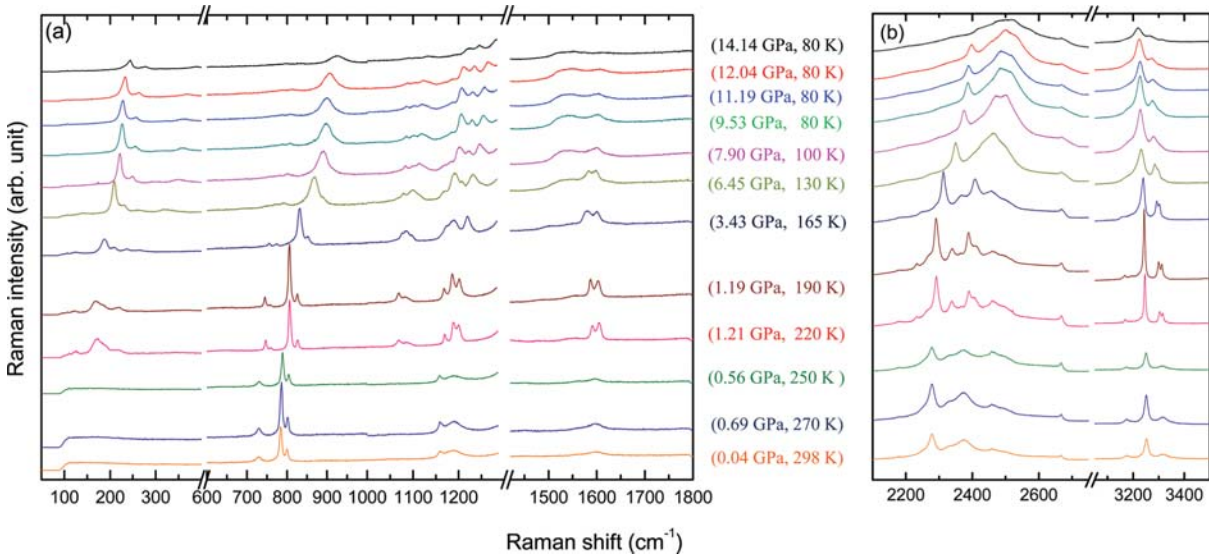

Figure 5. Selected Raman spectra during decompression and warming up processes from 14.14 GPa, 80 K to ambient pressure, room temperature. The (P, T) is labeled for each spectrum in the experimental sequence starting from the top and ending at the bottom.

Table 2. Factor Group Analysis of Vibrational Modes of NH_3BH_3 under Space Group $Cmc2_1$

Point group C_{3v} [a]	Site symmetry Cs	Factor group C_{2v}	Raman mode	Counts Predicted	Counts Observed[b]
$2\times5A_1$	10A'	$5A_1$	ν_1	2	1
			ν_2	2	1
			ν_3	2	– [c]
		$5B_2$	ν_4	2	1
			ν_5	2	1
$2\times6E$	12A'	$6A_1$	ν_7	4	2
			ν_8	4	3
		$6B_2$	ν_9	4	2
	12A"	$6A_2$	ν_{10}	4	3
			ν_{11}	4	4
		$6B_1$	ν_{12}	4	2

[a] The A_2 mode in C_{3v} symmetry is not Raman active. [b] The maximum number of components for each Raman mode (associated with the original C_{3v} molecular symmetry) in the pressure regions of >2 GPa. [c] The NH_3 deformation mode ν_3 (1377 cm^{-1}) was not monitored due to the intense Raman mode of the diamond.

each compression sequence was very different, i.e., a disordered tetragonal structure ($I4mm$) at room temperature versus an ordered orthorhombic structure ($Pmn2_1$) at 180 K. It is therefore of interest to understand the possible structures of the high-pressure phases at 180 K and their correlation with those at room temperature. This information, together with previously established room-temperature crystal structures will allow us to extend the phase diagram of NH_3BH_3 to temperatures down to 80 K and pressures up to 15 GPa.

On the basis of the similar Raman profiles of NH_3BH_3 in the pressure region <2 GPa at 180 K, it is reasonable to assign the structure in this pressure region (0−1.5 GPa) at 180 K with space group $Pmn2_1$, an extension of the ambient pressure structure below 225 K.[19] The significantly different lattice profile as well as the different degrees of splitting of the Raman internal modes of NH_3BH_3 in the subsequent higher pressure regions, however, suggests that the crystal structures of those phases were significantly different than $Pmn2_1$. So far, the known high-pressure phases (i.e., >1.5 GPa) at room temperature have another orthorhombic crystal lattice with space group $Cmc2_1$. Factor group analysis, a well-established method in vibrational spectroscopy for crystals that have been widely used in previous studies,[20,21] may help to justify the possible crystal structures of the new phase of NH_3BH_3. Assuming that the low-temperature (<225 K) and high-pressure (>2 GPa) phases have a similar orthorhombic structure, such as $Cmc2_1$, the result of the analysis is shown in Table 2. Starting with the molecular symmetry of C_{3v} with its irreducible representation shown in eq 1, by correlation with factor group C_{2v}^{12} (for $Cmc2_1$) with $Z = 4$ (and thus $Z' = 2$) via Wyckoff site of Cs symmetry, the irreducible representations of the internal modes and lattice modes of NH_3BH_3 that are Raman active are

$$\Gamma_{\text{internal}}^{Cmc2_1} = 11A_1 + 6A_2 + 6B_1 + 11B_2 \quad (3)$$

$$\Gamma_{\text{lattice}}^{Cmc2_1} = 2A_1 + 3A_2 + 2B_1 + 2B_2 \quad (4)$$

Apparently, the maximum number of observed lattice modes (e.g., three) was only a subset of the total of nine predicted Raman active lattice modes under space group $Cmc2_1$. In addition, each of the ν_1 to ν_5 modes individually was predicted to exhibit a doublet whereas modes ν_7 to ν_{12} should have had a quartet Raman profile under the assumed factor group. As a matter of fact, in each pressure region of 1.5−5, 5−8, and >8 GPa, the maximum number of observed Raman modes splitting was also less than those predicted except for the ν_{11} mode, which matched the prediction exactly (Table 2). Incomplete factor group splitting is very common and has been observed in Hess's low-temperature study of NH_3BH_3[19] as well as in other borohydride or amide materials.[20,21] Although there is no contradiction between the observed Raman profiles and the assumed factor group, other similar space groups cannot be ruled out. Detailed in situ

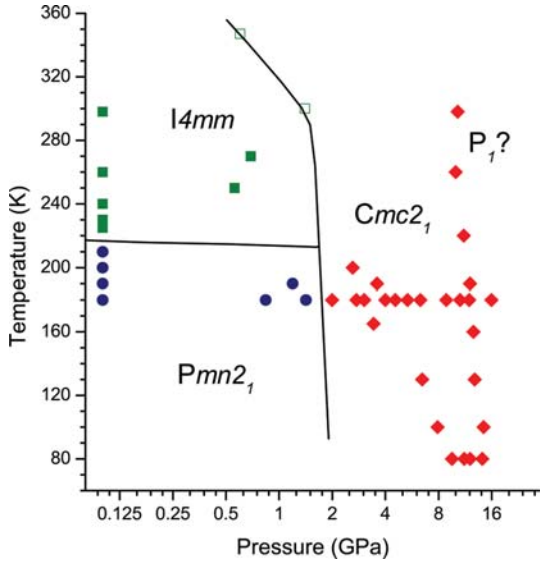

Figure 6. Schematic phase diagram of NH_3BH_3 in the pressure region of 0−15 GPa (in log 2 scale) and temperature region of 80−350 K. Solid symbols are experimental data from the current study, with squares for *I*4*mm* phase, circles for *Pmn*2$_1$ phase and diamonds for *Cmc*2$_1$ phase. The open squares are adopted from Chen's X-ray work (ref 29). The solid lines denote the rough boundaries among the three known phases. The *P*1 phase labeled is considered tentative (see text).

low-temperature and high-pressure X-ray diffraction measurements will help to elucidate the crystal structures of these phases.

An associated question is what is the nature of the phase transitions at 5 and 8 GPa and the relationship among these higher pressure phases. Vibrational spectroscopy provides sensitive information about molecular structures, the nature of bonding, and the intermolecular and intramolecular interactions. As a result, the reduction of intra- and/or intermolecular distances by compression may significantly enhance these interactions as evidenced by the Raman frequency shift, and intensity variation as well as the factor group splittings, even within the same or slightly modified crystal lattice. Therefore, these phase transitions identified by spectroscopy could be second-order phase transitions that may not correlate with the X-ray measurements exactly. For instance, although both Lin's and our previous spectroscopic studies suggested multiple phases of NH_3BH_3 at high pressures and room temperature,[24,27] later X-ray measurements and theoretical studies suggested that there was only one major phase transition involving the change of crystal structures from *I*4*mm* to *Cmc*2$_1$.[28,29] Thus, it is reasonable to believe that the phase transitions observed in the current low-temperature study may have similar origins as those observed at room temperature, and therefore, the stability regions of the previously observed high-pressure phases can be extended from room temperature to 80 K. Indeed, for example, the extremely similar Raman profile achieved in this study (e.g., at 8.83 GPa and 180 K from Figure 3) when compared to that from our previous room-temperature study (e.g., at 8.5 GPa from Figure 2 of ref 24) strongly supports this understanding. Moreover, the molecular dynamics simulations by Wang et al.[31] suggest that the *Cmc*2$_1$ phase can be obtained from the *Pmn*2$_1$ structure at high pressure and low temperature, strongly supporting our proposal.

By combining the data of multiple runs following different $P-T$ paths, we can draw a schematic phase diagram roughly outlining the regions of the three known structures: *I*4*mm*, *Pmn*2$_1$, and *Cmc*2$_1$, as shown in Figure 6. We note that although Chen's measurements[29] (open squares) suggested a simple negative T/P slope, our measurements showed that the slope was much less temperature independent below 220 K. Furthermore, from the recent combined X-ray, neutron and DFT studies of NH_3BH_3 at room temperature by Kumar et al.,[30] a monoclinic structure with space group *P*1 was proposed above 8 GPa, which was in excellent agreement with a phase boundary claimed in the current study. However, the lack of significant changes in the Raman patterns across this pressure point, especially no further splittings of the Raman modes, do not seem to corroborate a crystal structure with such a low symmetry and so many molecular units per primitive cell (i.e., $Z = 16$). We thus labeled this proposed structure in the phase diagram only tentatively. Nonetheless, the band broadening for all the Raman modes with the depletion of the major modes above 15 GPa and 180 K suggested that the transformation to an amorphous phase via a significant structural disordering was consistent with the X-ray measurements taken at room temperature by Chen et al.[29] Again, more detailed in situ experiments as well as ab initio calculations may help with the understanding of these observations.

CONCLUSIONS

By in situ Raman spectroscopy, we investigated the pressure−temperature induced structural transformations of NH_3BH_3 at pressures up to 15 GPa and temperatures down to 80 K. Upon isothermal compression at 180 K, NH_3BH_3 was found to undergo phase transitions at about 1.5, 5, and 8 GPa, in excellent alignment with those transitions observed at room temperature in our previous work. In addition, the pressure evolution of the Raman spectra across these transition boundaries as well as the pressure-dependence of major Raman modes follow a similar pattern to those observed at room temperature. Using factor group analysis, we found that the phases above 1.5 GPa were consistent with the crystal structure with space group *Cmc*2$_1$, although other possibilities cannot be ruled out. The transitions at 5 and 8 GPa are second order in nature and can be interpreted as enhanced intermolecular interactions within the same or possibly a slightly modified crystal lattice. Further compression above 15 GPa leads to the gradual transformation to an amorphous phase. Upon decompression and warming up, these $P-T$ induced phase transitions were found to be reversible. Raman data from additional runs following different $P-T$ paths allowed for the construction of the $P-T$ phase diagram of NH_3BH_3 where the stability regions of the three previously established structures could be outlined. Further experimental and theoretical investigations are required to justify these understandings.

AUTHOR INFORMATION

Corresponding Author

*E-mail: yang.song@uwo.ca.

ACKNOWLEDGMENT

The authors acknowledge funding support from a Discovery Grant, a Research Tools and Instruments Grant from the Natural Science and Engineering Research Council of Canada, a Leaders Opportunities Fund from the Canadian Foundation for Innovation, an Early Research Award from the Ontario Ministry of

Research and Innovation, and a Petro-Canada Young Innovator Award from the University of Western Ontario.

REFERENCES

(1) Hamilton, C. W.; Baker, R. T.; Staubitz, A.; Manners, I. *Chem. Soc. Rev.* **2009**, *38*, 279.
(2) Staubitz, A.; Robertson, A. P. M.; Manners, I. *Chem. Rev.* **2010**, *110*, 4079.
(3) Stephens, F. H.; Pons, V.; Baker, R. T. *Dalton Trans.* **2007**, 2613.
(4) Yang, J.; Sudik, A.; Wolverton, C.; Siegel, D. J. *Chem. Soc. Rev.* **2010**, *39*, 656.
(5) Satyapal, S.; Petrovic, J.; Read, C.; Thomas, G.; Ordaz, G. *Catal. Today* **2007**, *120*, 246.
(6) Chellappa, R. S.; Autrey, T.; Somayazulu, M.; Struzhkin, V. V.; Hemley, R. J. *ChemPhysChem* **2010**, *11*, 93.
(7) Li, Z. Y.; Zhu, G. S.; Lu, G. Q.; Qiu, S. L.; Yao, X. D. *J. Am. Chem. Soc.* **2010**, *132*, 1490.
(8) Osborn, W.; Sadowski, T.; Shaw, L. L. *Scr. Mater.* **2011**, *64*, 737.
(9) Zhang, Y.; Shimoda, K.; Ichikawa, T.; Kojima, Y. *J. Phys. Chem. C* **2010**, *114*, 14662.
(10) Xiong, Z. T.; Yong, C. K.; Wu, G. T.; Chen, P.; Shaw, W.; Karkamkar, A.; Autrey, T.; Jones, M. O.; Johnson, S. R.; Edwards, P. P.; David, W. I. F. *Nat. Mater.* **2008**, *7*, 138.
(11) Allis, D. G.; Kosmowski, M. E.; Hudson, B. S. *J. Am. Chem. Soc.* **2004**, *126*, 7756.
(12) Cho, H.; Shaw, W. J.; Parvanov, V.; Schenter, G. K.; Karkamkar, A.; Hess, N. J.; Mundy, C.; Kathmann, S.; Sears, J.; Lipton, A. S.; Ellis, P. D.; Autrey, S. T. *J. Phys. Chem. A* **2008**, *112*, 4277.
(13) Dillen, J.; Verhoeven, P. *J. Phys. Chem. A* **2003**, *107*, 2570.
(14) Dixon, D. A.; Gutowski, M. *J. Phys. Chem. A* **2005**, *109*, 5129.
(15) Kathmann, S. M.; Parvanov, V.; Schenter, G. K.; Stowe, A. C.; Daemen, L. L.; Hartl, M.; Linehan, J.; Hess, N. J.; Karkamkar, A.; Autrey, T. *J. Chem. Phys.* **2009**, *130*, 024507.
(16) Bowden, M. E.; Gainsford, G. J.; Robinson, W. T. *Aust. J. Chem.* **2007**, *60*, 149.
(17) Hughes, E. W. *J. Am. Chem. Soc.* **1956**, *78*, 502.
(18) Klooster, W. T.; Koetzle, T. F.; Siegbahn, P. E. M.; Richardson, T. B.; Crabtree, R. H. *J. Am. Chem. Soc.* **1999**, *121*, 6337.
(19) Hess, N. J.; Bowden, M. E.; Parvanov, V. M.; Mundy, C.; Kathmann, S. M.; Schenter, G. K.; Autrey, T. *J. Chem. Phys.* **2008**, *128*, 4508.
(20) Liu, A.; Song, Y. *J. Phys. Chem. B* **2011**, *115*, 7.
(21) Liu, A.; Xie, S. T.; Dabiran-Zohoory, S.; Song, Y. *J. Phys. Chem. C* **2010**, *114*, 11635.
(22) Murli, C.; Song, Y. *J. Phys. Chem. B* **2009**, *113*, 13509.
(23) Song, Y.; Murli, C.; Liu, Z. X. *J. Chem. Phys.* **2009**, *131*, 174506.
(24) Xie, S. T.; Song, Y.; Liu, Z. X. *Can. J. Chem.* **2009**, *87*, 1235.
(25) Custelcean, R.; Dreger, Z. A. *J. Phys. Chem. B* **2003**, *107*, 9231.
(26) Trudel, S.; Gilson, D. F. R. *Inorg. Chem.* **2003**, *42*, 2814.
(27) Lin, Y.; Mao, W. L.; Drozd, V.; Chen, J. H.; Daemen, L. L. *J. Chem. Phys.* **2008**, *129*, 234509.
(28) Filinchuk, Y.; Nevidomskyy, A. H.; Chernyshov, D.; Dmitriev, V. *Phys. Rev. B* **2009**, *79*, 214111.
(29) Chen, J. H.; Couvy, H.; Liu, H. Z.; Drozd, V.; Daemen, L. L.; Zhao, Y. S.; Kao, C. C. *Int. J. Hydrogen Energy* **2010**, *35*, 11064.
(30) Kumar, R. S.; Ke, X. Z.; Zhang, J. Z.; Lin, Z. J.; Vogel, S. C.; Hartl, M.; Sinogeikin, S.; Daemen, L.; Cornelius, A. L.; Chen, C. F.; Zhao, Y. S. *Chem. Phys. Lett.* **2010**, *495*, 203.
(31) Wang, L. C.; Bao, K.; Meng, X.; Wang, X. L.; Jiang, T. T.; Cui, T. A.; Liu, B. B.; Zou, G. T. *J. Chem. Phys.* **2011**, *134*, 024517.
(32) Strobel, T. A.; Somayazulu, M.; Hemley, R. J. *Phys. Rev. Lett.* **2009**, *103*, 065701.
(33) Chellappa, R. S.; Somayazulu, M.; Struzhkin, V. V.; Autrey, T.; Hemley, R. J. *J. Chem. Phys.* **2009**, *131*, 224515.
(34) Lin, Y.; Mao, W. L.; Mao, H. K. *Proc. Natl. Acad. Sci. U.S.A.* **2009**, *106*, 8113.
(35) Mao, W. L.; Mao, H. K.; Goncharov, A. F.; Struzhkin, V. V.; Guo, Q. Z.; Hu, J. Z.; Shu, J. F.; Hemley, R. J.; Somayazulu, M.; Zhao, Y. S. *Science* **2002**, *297*, 2247.
(36) Wang, S. B.; Mao, W. L.; Autrey, T. *J. Chem. Phys.* **2009**, *131*, 144508.
(37) Wang, S. B.; Mao, H. K.; Chen, X. J.; Mao, W. L. *Proc. Natl. Acad. Sci. U.S.A.* **2009**, *106*, 14763.
(38) Ragan, D. D.; Gustavsen, R.; Schiferl, D. *J. Appl. Phys.* **1992**, *72*, 5539.
(39) Yen, J.; Nicol, M. *J. Appl. Phys.* **1992**, *72*, 5535.